PUBLICATIONS OF THE ASTRONOMICAL SOCIETY OF THE PACIFIC, **118**:2–20, 2006 January

The Carnegie Supernova Project: The Low-Redshift Survey

MARIO HAMUY,[1] GASTÓN FOLATELLI, NIDIA I. MORRELL, AND MARK M. PHILLIPS

Carnegie Institution of Washington, Las Campanas Observatory, Colina El Pino s/n, Casilla 601, La Serena, Chile

NICHOLAS B. SUNTZEFF

Cerro Tololo Inter-American Observatory, National Optical Astronomy Observatory,[2] Casilla 603, La Serena, Chile

S. E. PERSSON

Carnegie Institution of Washington, 813 Santa Barbara Street, Pasadena, CA 91101

MIGUEL ROTH, SERGIO GONZALEZ, WOJTEK KRZEMINSKI, AND CARLOS CONTRERAS

Carnegie Institution of Washington, Las Campanas Observatory, Colina El Pino s/n, Casilla 601, La Serena, Chile

WENDY L. FREEDMAN, D. C. MURPHY, BARRY F. MADORE, AND P. WYATT

Carnegie Institution of Washington, 813 Santa Barbara Street, Pasadena, CA 91101

JOSÉ MAZA

Departamento de Astronomía, Universidad de Chile, Casilla 36-D, Santiago, Chile

ALEXEI V. FILIPPENKO AND WEIDONG LI

Department of Astronomy, University of California, 601 Campbell Hall 3411, Berkeley, CA 94720-3411

AND

P. A. PINTO

Steward Observatory, University of Arizona, Tucson, AZ 85721

Received 2005 September 30; accepted 2005 December 1; published 2006 January 6

ABSTRACT. Supernovae are essential to understanding the chemical evolution of the universe. Type Ia supernovae also provide the most powerful observational tool currently available for studying the expansion history of the universe and the nature of dark energy. Our basic knowledge of supernovae comes from the study of their photometric and spectroscopic properties. However, the presently available data sets of optical and near-infrared light curves of supernovae are rather small and/or heterogeneous, and employ photometric systems that are poorly characterized. Similarly, there are relatively few supernovae whose spectral evolution has been well sampled, both in wavelength and phase, with precise spectrophotometric observations. The low-redshift portion of the Carnegie Supernova Project (CSP) seeks to remedy this situation by providing photometry and spectrophotometry of a large sample of supernovae taken on telescope/filter/detector systems that are well understood and well characterized. During a 5 year program that began in 2004 September, we expect to obtain high-precision $u'g'r'i'BVYJHK_s$ light curves and optical spectrophotometry for about 250 supernovae of all types. In this paper we provide a detailed description of the CSP survey observing and data reduction methodology. In addition, we present preliminary photometry and spectra obtained for a few representative supernovae during the first observing campaign.

1. INTRODUCTION

A universe dominated by normal mass should undergo deceleration as it expands. Thus, the counterintuitive discovery of an accelerating universe based on observations of Type Ia supernovae (Riess et al. 1998; Perlmutter et al. 1999) is of profound significance for physics. Evidently "dark energy," in the form of Einstein's cosmological constant or a more general scalar energy field, is the dominant mass/energy constituent of the universe today.

These important implications depend critically on the quality of the light curves of the Type Ia supernovae (SNe Ia) and the ability to *K*-correct, deredden, and normalize these to a standard luminosity. The evidence for an accelerating universe is based on a differential measurement between local and distant SNe

[1] Current address: Departamento de Astronomía, Universidad de Chile, Casilla 36-D, Santiago, Chile; mhamuy@das.uchile.cl.

[2] Cerro Tololo Inter-American Observatory, National Optical Astronomy Observatory, operated by the Association of Universities for Research in Astronomy, Inc., under cooperative agreement with the National Science Foundation.

Ia (at look-back times of 4–10 Gyr). The local samples are very heterogeneous, and as more SNe have been added, the full sample dispersion around the local Hubble flow has increased from 0.12 (Phillips et al. 1999) to 0.18 mag (Jha 2002) in units of distance modulus. Moreover, there are still legitimate concerns about possible systematic errors due to poorly understood photometric systems (Suntzeff 2000; Stritzinger et al. 2002), reddening corrections (Phillips et al. 1999), and evolutionary effects (Hamuy et al. 2000; Gallagher et al. 2005). A new and larger sample of nearby ($z < 0.07$) SNe, where these sources of observational error have been duly accounted for, is urgently needed.

With that purpose in mind, we have initiated a 5 year program, the Carnegie Supernova Project (CSP), to obtain well-calibrated optical and near-infrared (NIR) light curves, as well as optical spectrophotometry of ~250 Type Ia and core-collapse SNe. The CSP is built upon the unique resources of the Las Campanas Observatory (LCO) in Chile. We have guaranteed access to large numbers of nights on the Swope 1 m and the du Pont 2.5 m telescopes (~300 per year in both telescopes together), which are equipped with high-performance CCD optical imagers, NIR cameras, and CCD optical spectrographs. In addition to providing densely sampled light curves covering the near-ultraviolet to the NIR ($u'g'r'i'BVYJHK_s$), we have the means to obtain optical spectrophotometry at approximately weekly intervals. The CSP is a follow-up project and relies on SNe discovered in the course of other surveys. A large fraction of our targets come from the Lick Observatory Supernova Search (LOSS; Li et al. 2000; Filippenko et al. 2001; Filippenko 2003, 2005) conducted with the Katzman Automatic Imaging Telescope (KAIT), and from dedicated SN searches by amateur astronomers (e.g., T. Puckett, T. Boles, B. Monard, K. Itagaki), which constitute a growing source of nearby SNe. The targets selected for the follow-up observations by the CSP are SNe discovered before or near maximum light with $z \lesssim 0.07$ and $\delta \lesssim +20°$.

The primary goal of the CSP is to establish a fundamental data set of optical and NIR light curves in a well-defined and well-understood photometric system for all types of SNe. A secondary goal is to obtain complementary optical spectrophotometry for these same SNe. The data set for the Type Ia events will allow us to improve extinction corrections and to investigate systematic effects possibly due to differences in age and metallicity. The data for the Type II SNe will be used to establish and refine precise techniques for measuring luminosity distances employing the Expanding Photosphere Method (Eastman et al. 1996; Schmidt et al. 1994; Hamuy et al. 2001; Leonard et al. 2002; Dessart & Hillier 2005) or the Standardized Candle Method (Hamuy & Pinto 2002), thereby providing an independent check on the Type Ia results. We will be able to explore the use of both SN types for studies of local galaxy flows and independently measure the convergence depth (the distance at which the bulk flows smooth out into the so-called large-scale Hubble flow). Ultimately, the data set will serve as a reference for observations of distant SNe that will be obtained in coming years in the course of the Joint Dark Energy Mission (Aldering 2005) and those being obtained in the course of the high-z SN surveys such as the Canada-France-Hawaii Telescope Legacy project (Pritchet 2005), ESSENCE (Matheson et al. 2005), and our own high-z component of the CSP, which seeks to measure rest-band I magnitudes of SNe Ia at $z \approx 0.5$ using the Magellan telescopes (Freedman 2005).

The low-z CSP data set will also allow us to gain a deeper understanding of the physics of thermonuclear (Type Ia) events and the different classes of core-collapse SNe (Types II, Ib, Ic). For example, during the first CSP observing campaign, we obtained excellent coverage of SN 2005bf, a peculiar, luminous Type Ic event that peaked 35 days after explosion and that may represent a transition object between the SNe associated with gamma-ray bursts and ordinary SNe Ib (Folatelli et al. 2006).

The purpose of this paper is to describe the low-z CSP experiment, to explain the general procedures for data acquisition and reduction, to summarize the results obtained during the first (2004–2005) low-z CSP observing campaign, and to present the data for a few representative SNe. In § 2 we discuss the instrumentation, in § 3 we describe our observations, in § 4 we explain the data reduction procedures, and in § 5 we show representative light curves and spectra obtained thus far.

2. TELESCOPES, INSTRUMENTS, AND PHOTOMETRIC SYSTEMS

A large fraction of our targets come from LOSS, which discovers approximately 50% of the low-z SNe found annually. Although LOSS is conducted at northern latitudes, in 2004 the search was adjusted to include more galaxies south of the celestial equator and thus accessible to the Carnegie telescopes. Over half of the current LOSS SNe are located south of $\delta = +20°$ and are observable from LCO. The discovery redshift limit, $z \lesssim 0.05$, of the LOSS SNe is ideally matched to the telescopes and detectors available to the CSP. The rest of the targets come from a variety of searches carried out by amateur astronomers at different observatories. The telescopes employed to date for the CSP are the Swope 1.0 m, the du Pont 2.5 m, and to a lesser extent the Magellan 6.5 m telescopes at LCO. In addition, some spectra have been obtained with the 1.5 m telescope at Cerro Tololo Inter-American Observatory (CTIO). Various telescopes at Lick Observatory have also been used for photometry and spectroscopy (e.g., Foley et al. 2003), but those observations will be described in separate papers.

In the remainder of this section, we describe the instrumentation used with these telescopes. Table 1 lists the instruments used for the low-z CSP.

TABLE 1
INSTRUMENTS USED FOR THE LOW-z CSP

Telescope	Instrument	Detector	Plate Scale (arcsec pixel^{-1})	Filters or $\Delta\lambda$ (Å)	Photometry/ Spectroscopy?
Swope	CCD Camera	SITe 2048 × 3150 ("Site 3")	0.435	$u'g'r'i'BV$	Photometry
du Pont	WFCCD	Tek 2048 × 2048 ("TEK 5")	0.774	BVI	Photometry
	CCD Camera	Tek 2048 × 2048 ("TEK 5")	0.259	$u'g'r'i'BV$	Photometry
Clay	LDSS-2	SITe 2048 × 2048 ("Site 1")	0.380	BVR	Photometry
	LDSS-3	STA 4064 × 4064 ("STAO500A")	0.190	$Bg'r'i'$	Photometry
Swope	RetroCam	HAWAII-1 1024 × 1024	0.540	YJH	Photometry
du Pont	WIRC	HAWAII-1 1024 × 1024	0.196	$YJHK_s$	Photometry
Baade	PANIC	HAWAII-1 1024 × 1024	0.125	$YJHK_s$	Photometry
du Pont	WFCCD	Tek 2048 × 2048 ("TEK 5")	0.774	3800–9200	Spectroscopy
	Modular Spectrograph	SITe 1752 × 572 ("Site 2")	0.350	3780–7270	Spectroscopy
Clay	LDSS-2	SITe 2048 × 2048 ("Site 1")	0.380	3600–9000	Spectroscopy
CTIO 1.5 m	RC Spectrograph	Loral 1200 × 800	0.270	3000–10100	Spectroscopy

NOTE.—Additional data are obtained at Lick Observatory with KAIT, the Nickel 1 m reflector, and the Shane 3 m telescope; see, e.g., Foley et al. (2003).

2.1. Optical Imaging

The vast majority of the CSP optical imaging is being obtained with the Swope 1 m f/7 telescope Direct CCD Camera, which uses a 2048 × 3150 pixel, 15 μm pixel^{-1} SITe CCD. This detector has a readout noise of 6.6 e^- and a gain of 2.5 e^- ADU^{-1} (where ADU means analog-to-digital converter unit). To speed up the CCD readout and save disk space, we limit the readout to 1200 × 1200 pixels. At a scale of 0.″435 pixel^{-1}, this corresponds to a field of view (FOV) of 8.′7 × 8.′7. The quality of images obtained at the Swope telescope ranges from ~1″ to 2″ FWHM, with an average seeing of 1.″3.

For our optical passbands we utilize Sloan Digital Sky Survey (SDSS) $u'g'r'i'$ filters, in addition to Johnson B and V filters (Fukugita et al. 1996; Bessell 1990). We have chosen SDSS filters because we feel it is likely that this will be the dominant photometric filter set for the next decade due to the all-sky photometric maps of the SDSS (north) and the Mount Stromlo and Siding Spring Observatories SkyMapper[3] project (south). We decided not to use the z' filter because the red side of the filter is determined by the CCD quantum efficiency (QE) and not solely by the filter bandpass. The CCD red response is very temperature sensitive, causing the combined filter-plus-detector throughput to be variable. The z' bandpass also overlaps with a saturated H_2O band at 9300 Å, adding further uncertainty to its total throughput and effective wavelength. The B and V filters were included in our program to sample the spectral region covered by the g' filter with somewhat narrower filters and to facilitate comparison of our results with historical data sets.

Our SDSS filters were manufactured by Asahi Spectra Company, Ltd.,[4] as specified in Table 2. We have synthesized natural-system passbands by combining the filter transmissions with the CCD QE, two aluminum reflectivity curves (one for the primary and another for the secondary mirror), and an atmospheric transmission spectrum. The resulting SDSS bandpasses are shown in the top panel of Figure 1, along with the standard bandpasses (normalized at maximum) for the USNO 40 inch (1 m) telescope. This comparison reveals an excellent match between the two systems, with the exception that our i' bandpass is somewhat narrower than that used at the USNO;

[3] See http://msowww.anu.edu.au/skymapper.

[4] This is the same company that built the filters used with the USNO 40 inch telescope for the establishment of the SDSS photometric system (Smith et al. 2002).

TABLE 2
SPECIFICATIONS FOR THE SDSS AND JOHNSON FILTERS

Filter	Instrument	Specifications
u'	Swope CCD Camera	AR*KG5 (2 mm) + UG11 (1 mm) + fused silica (3 mm) + fused silica (4 mm)*IF
g'	Swope CCD Camera	AR*GG400 (2 mm) + BG40 (2 mm) + BK7 (6 mm)*IF
r'	Swope CCD Camera	AR*OG550 (4 mm) + BK7 (6 mm)*IF
i'	Swope CCD Camera	AR*RG695 (4 mm) + BK7 (6 mm)*IF
B	Swope CCD Camera	GG385 (2 mm) + BG12 (1 mm) + S8612 (2 mm)
V	Swope CCD Camera	GG495 (2 mm) + S8612 (3 mm)
B	Clay LDSS-2	BG12 (1 mm) + BG39 (2 mm) + GG385 (1 mm)
V	Clay LDSS-2	GG495 (2 mm) + BG39 (2 mm)
R	Clay LDSS-2	OG570 (2 mm) + KG3 (2 mm)

NOTE.—AR = Antireflection coating; IF = interference film.

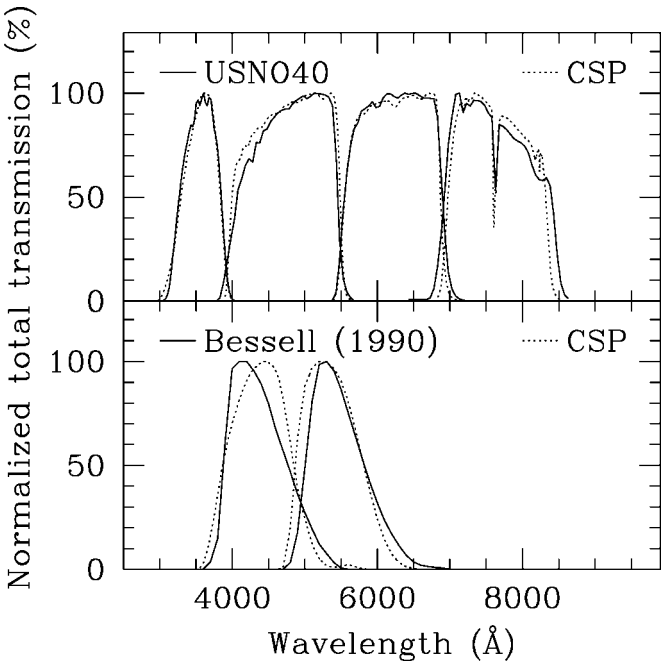

FIG. 1.—*Top*: Natural-system synthetic bandpasses for the Swope $u'g'r'i'$ SDSS filters (*dotted lines*) and the USNO 40 inch telescope standard bandpasses (*solid lines*) used for the establishment of the SDSS photometric system (normalized to 100% at maximum). *Bottom*: Natural-system bandpasses for the Swope Harris *B* and *V* filters (*dotted lines*) and the *B* and *V* Bessell (1990) bandpasses (divided by a linear function in wavelength and normalized to 100% at maximum).

the effective wavelength is, however, unchanged. The bottom panel of Figure 1 compares the passbands for our Harris *B* and *V* filters with the Johnson *B* and *V* passbands described by Bessell (1990). It is clear that our instrumental system provides a reasonable match to the Johnson system.

Since one of our goals is to eliminate systematic errors in the SN magnitudes caused by differences between the instrumental and the standard bandpasses, we have started a program of regular measurements of the transmission of our filters using a spectrometer at LCO. Similarly, we are planning in the near future to improve the measurement of the QE curve for the Swope CCD using equipment available for this purpose at the CTIO laboratories. Our natural-system bandpasses will be regularly updated as we improve our measurements of the CCD QE, the mirror reflectivities, and other optical elements of our instrument. All of these will be posted on the CSP World Wide Web site and made available through the NASA/IPAC Extragalactic Database (NED).

Some *BVI* imaging has also been obtained with the Wide Field Reimaging CCD Camera (WFCCD) on the 2.5 m f/7.5 du Pont telescope. This uses a 2048 × 2048 pixel Tektronix CCD with 24 μm pixels. A subraster is used to observe a $23' \times 13'$ FOV at a scale of $0''.774$ pixel^{-1}.

Likewise, a small amount of *BVR* imaging has been taken with the Low-Dispersion Survey Spectrograph (LDSS-2; Allington-Smith et al. 1994) on the 6.5 m f/11 Magellan Clay telescope. Until the end of 2004, this instrument employed a SITe CCD for which we limited the readout to a section of 2048 × 1240 pixels containing a circular FOV of $6'.4$ diameter. The pixel size of 15 μm corresponds to a scale of $0''.38$ pixel^{-1}. The *BVR* filter specifications for this instrument are given in Table 2. In 2005 February, the LDSS-2 instrument underwent a significant upgrade that involved replacement of both the optics and the detector. The new CCD is an STA0500A detector with 4064 × 4064 pixels that, in combination with the new optics, has a scale of $0''.19$ pixel^{-1}. The upgraded instrument, now called LDSS-3, retains the same *B* filter used in LDSS-2, but the *V* and *R* filters were replaced by SDSS g', r', i', and z' filters. Although we have not yet employed LDSS-3 for the CSP, we expect to do so occasionally in the future.

For galaxy subtraction, we need template images after the SN has faded. These will be obtained beginning in 2005 November with the Direct CCD Camera on the 2.5 m du Pont telescope. The detector is the same one used with the WFCCD and covers a FOV of $8'.8 \times 8'.8$ with a scale of $0''.259$ pixel^{-1}. With a typical image quality of $0''.7$ (FWHM) at the du Pont telescope, this instrument is ideal for acquiring high-quality deep templates. The filter set will be the same as that used on the 1 m telescope.

2.2. Infrared Imaging

During the first CSP campaign, we obtained 85% of the NIR images with the Wide Field Infrared Camera (WIRC) on the 2.5 m du Pont telescope (Persson et al. 2002), but this situation will change when a new NIR camera, RetroCam, becomes available at the Swope telescope for the second campaign (see § 6). WIRC is equipped with four 1024 × 1024 pixel Rockwell HAWAII-1 HgCdTe arrays forming a 2 × 2 square footprint with a $175''$ center-to-center spacing in the reimaged telescope focal plane. Each array covers a FOV of $\sim 3'.3 \times 3'.3$ with a $0''.196$ pixel^{-1} scale. For SN imaging we use the two best quality detectors of the four (detectors 2 and 3). Departures from linearity in measured flux are 1% below 30,000 e^-, growing to about the 5% level at $\sim$60,000 e^- (see § 4.2). The typical image quality for this instrument falls between $0''.5$ and $0''.8$ (FWHM). We observe in the *Y*, *J*, *H*, and K_s passbands, using filters manufactured by Barr Associates, Ltd. (*Y*, *J*, *H*), and Optical Coating Laboratory, Inc. (K_s).

Some NIR data have also been obtained using the Persson Auxiliary Nasmyth Infrared Camera (PANIC) mounted on the 6.5 m Baade telescope (Martini et al. 2004). This instrument has a single 1024 × 1024 pixel HgCdTe HAWAII-1 detector covering a $2' \times 2'$ FOV at a scale of $0''.125$ pixel^{-1}. The nonlinear behavior of the detector is similar to that of the WIRC arrays. The active optics on the primary mirror produce a typical image quality of $0''.3$–$0''.6$ (FWHM). The *Y*, *J*, *H*, and K_s filters are similar to those employed with WIRC.

Figure 2 shows the total system transmission curves for WIRC and PANIC, with the $YJHK_s$ filters. The plotted curves include atmospheric transmission, throughput of every optical element in the telescope and instrument, and detector QE. The graph shows excellent agreement between the WIRC and PANIC systems.

2.3. Spectroscopy

The majority of our spectroscopic observations have been obtained with the 2.5 m du Pont telescope using the WFCCD instrument in its spectroscopic long-slit mode. A 400 line mm^{-1} blue grism is employed with the Tektronix 2048 × 2048 pixel CCD to provide a wavelength coverage from 3800 to 9200 Å at a dispersion of 3.0 Å pixel^{-1}. For the ∼1.″6 slit width used for the SN observations, this setup gives a FWHM resolution of ∼6.0 Å. For a $V = 16$ mag object in clear conditions, a signal-to-noise ratio (S/N) per pixel of 50 at 5000 Å is typically achieved for an exposure time of 1200 s.

When the WFCCD is not available on the 2.5 m telescope due to block scheduling constraints, it has been possible to obtain some spectra with the Las Campanas Modular Spectrograph. This instrument uses a SITe 1752 × 572 pixel CCD with 15 μm pixel^{-1} and a 300 line mm^{-1} grating (blazed at 5000 Å). The resulting spectral coverage is ∼3800–7300 Å at a dispersion of 2.45 Å pixel^{-1}. A slit width of 1″ is used for the SN observations, which gives a FWHM resolution of ∼7 Å. Compared to the WFCCD, this instrument has lower efficiency and longer exposures are required.

Occasionally during the first CSP campaign, we were scheduled single nights at the 6.5 m Magellan Clay telescope with LDSS-2. For these observations, a 300 line mm^{-1} grism blazed at 5000 Å was employed, providing wavelength coverage of 3600–9000 Å at a dispersion of 5.3 Å pixel^{-1}. For a 1″ slit, this translates to a FWHM resolution of ∼13.5 Å.

Approximately 10% of the CSP spectroscopy has been carried out with the CTIO 1.5 m telescope in the service mode of the SMARTS consortium.[5] We use the facility Ritchey-Chrétien (RC) Cassegrain Spectrograph equipped with a 1200 × 800 pixel Loral CCD, usually at $R = 300$, which gives a dispersion of 5.7 Å pixel^{-1}, a wavelength coverage of 3000–10100 Å, and a FWHM resolution of ∼14 Å.

Note that for none of the above spectrographs do we employ a filter to block second-order light, which means that there could be second-order contamination redward of about 7000 Å. This effect will be quantified in a future paper.

3. OBSERVATIONS

Our plan is to carry out an intensive 9 month campaign each year, September through May, for 5 years. The extended nature of each campaign allows us to follow SNe discovered before the end of month seven (March). Given that various searches are currently producing ∼100 southern low-z SNe per year, we expect complete light-curve coverage for ∼50 SNe (25 SNe Ia, 20 SNe II, and 5 SNe Ibc) for each 9 month campaign. Our observational goals are (1) for SNe Ia and SNe Ibc, to acquire $u'g'r'i'BVYJHK_s$ photometry to 0.03 mag precision (random error) every 3–4 days and optical spectroscopy every 5–7 days from discovery through 50 days past maximum; (2) for SNe II, the same, except for additional coverage through the ∼100 day extended-plateau phase and onset of the nebular phase, but with a cadence of 7–10 days.

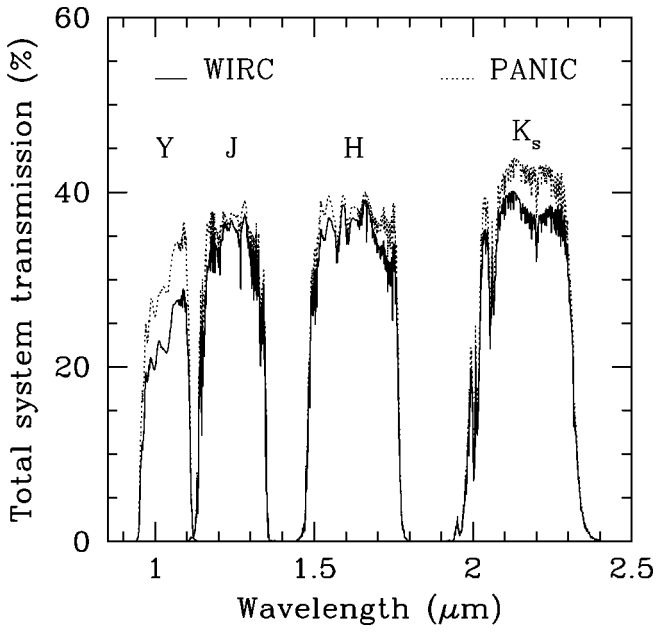

FIG. 2.—Total transmission curves for $YJHK_s$ in WIRC and PANIC. The curves include the Earth's atmosphere, the telescope and instrument optical elements, and the detector QE.

We collected data with no major interruption during our first campaign between 2004 September and 2005 May. During this period, the CSP was allocated 190 nights on the 1 m telescope for optical imaging. We also had 57 nights on the 2.5 m telescope, of which 33 were for NIR imaging, 19 for optical spectroscopy, and 5 for optical imaging. Strict observing procedures were established in order to obtain the data in the most homogeneous manner possible.

As soon as a report of a SN candidate was received, we triggered the follow-up program to begin generally the same night, even without a spectroscopic type or age. If a spectrum later revealed that the SN had been caught after maximum light, we dropped the object from our list of targets. Sometimes it took a while ($\lesssim$2 weeks) to obtain the SN spectrum, and in such cases, we used the photometric information collected by us to evaluate its probable type or age. For these purposes we devised a pipeline to produce preliminary light curves. At any given time we generally had 15 objects on our target list.

We have divided the labor of our project into three working

[5] See http://www.astro.yale.edu/smarts.

groups, each one having two individuals responsible for (1) keeping the observing instructions and procedures up to date, (2) sending the prioritized list of targets to the observers, (3) developing data reduction software, and (4) reducing the data immediately following the night. Observers were responsible for (1) checking the observing program for the night, (2) taking data and calibration images, (3) saving the data on storage media, (4) preparing a nightly observing report, and (5) updating the observing log for each SN. A fluid interaction and communication between the working group leader and the observers allowed us to optimize the telescope time, detect problems with the instrumentation, obtain excellent data, and reduce them promptly.

We designed and implemented a Web site for the project,[6] and the SN list, finding charts, observing procedures, observing programs, data reduction manuals, and many useful tools are available there. This Web site, where the photometric evolution of the objects we are following can be seen, is also open to the public.

In what follows we describe the specific observations that each of the working groups gathered during the first low-*z* CSP campaign.

3.1. Optical Imaging

Optical imaging with the 1 m Swope telescope would typically begin during the daytime by taking bias frames, as well as dome flats for each of the $g'r'i'BV$ filters with exposure times chosen to achieve ~23,000 e^- per pixel. Immediately after sunset, we would observe the twilight sky with the u' filter, followed by sky flats with two or three additional filters. Generally, three to five images were obtained per filter, making sure to offset the telescope between the individual images. The telescope was then focused using the V filter. For the remaining five filters, we would use previously derived focus offsets relative to the V filter.

During the night, SNe were observed according to the priorities previously assigned by the head of the optical-imaging working group, who determined exposure times based on the source brightness (typically 15 mag $\lesssim V \lesssim$ 20 mag) and our requirement to achieve 3% photometry. In general we would observe the SNe in all six filters, taking one image per filter. However, given that we usually had more objects to observe than telescope time available, we would drop the 3% precision requirement for the faintest objects and, in such cases, limit the exposure time to 900 s. When the resulting photometric precision reached 0.2 mag, we discontinued the observations through that filter. This would happen first in the u' filter, typically at a magnitude of ~21.

Johnson and SDSS standards (Landolt 1992; Smith et al. 2002) were observed regularly during photometric nights. At the beginning of the first campaign, few science targets were available so we observed 11–13 standard fields per night. As the campaign unfolded and more targets became active, we limited these observations to 4–5 fields. In all cases, we spread the observations of the standards over an air mass range of 1–2 for extinction determinations. The exposure times were 3–120 s depending on the filter used and the brightnesses of the stars. The purpose of these observations was to calibrate local standard stars in the field of each SN so that later on we could do differential photometry of the SN relative to them.

During cloudy nights, we performed detailed shutter timing and linearity tests on the Swope telescope. The results can be found in Appendices A and B.

The observations with WFCCD and LDSS-2 were performed in a way similar to those with the Swope telescope, except that we did not observe standard stars. We expect to observe standard fields in the future with the purpose of deriving color terms for the filters used. We did not measure the CCD responses and the shutter corrections for these instruments, but we expect to do so in the future for the WFCCD (the LDSS-2 is no longer operational).

3.2. Infrared Imaging

Calibration images for WIRC and PANIC were usually taken just after closing the dome at the end of the night. Typically the observer would obtain 15 dark frames with exposure times matching those of the science objects, 15 dome flats per filter with the dome lights on (with ~20,000 e^- pixel^{-1}), followed by 15 dome flats with the lights off. Final dome flats were constructed from the "lights-on" images minus the "lights-off" images. This procedure was found to be preferable, especially at K_s, to using dark-subtracted lights-on dome flats since contributions to the flux from additive sources were removed correctly. The latter sources include the camera window, telescope mirrors, and scattered thermal emission, which illuminate the detector differently than does the flat-field screen.

For WIRC, we obtained twilight flats on some nights to test the illumination quality of the dome flats. These tests showed agreement between twilight and dome flats within 1% for all four NIR passbands. However, for PANIC it was necessary to take twilight flats for illumination corrections to bring the photometric flatness to better than 2%. We took twilight flats every night in sets of at least five exposures per filter, offsetting the telescope between exposures and controlling the flux level to be in the linear regime. We used dome flats for both WIRC and PANIC to build bad-pixel masks for each night.

For the WIRC observations, we preselected the telescope pointing for each SN such that there were a number of good local calibration stars in the field. Thus the SN was not always centered in the detector. We started observing each SN by placing it on detector 2 and taking a sequence of dithered exposures in one of the filters. Usually we used nine dither positions in a 3 × 3 square pattern, but when the SN was bright enough we used only five positions. We set the exposure time of the individual images to 20, 30, or 45 s, depending on the

[6] See http://csp1.lco.cl/~cspuser1.

brightness of the SN. Occasionally, for the faintest SNe we repeated the exposures at each dither position. Once the dither sequence was completed, we would offset the SN field to detector 3 and repeat the sequence for the same filter. This procedure allowed us to obtain sky images suitable for subtraction for each of the two detectors while observing the object on the other detector. We usually observed with all four filters, although in the case of faint SNe, we dropped the K_s filter because of the large uncertainties introduced by the high background levels that characterize this band. Typical times spent on each target, including overhead, were between 1 and 2 hr, with effective exposures between 200 and 800 s in each filter.

There are advantages and weaknesses to this technique. The advantage is that the nearby galaxies tend to be very large, making it generally impossible to use the median of the dithered SN+galaxy data on a single detector to form a clean sky image with no print-through. The sequence of off-source dithered exposures (obtained when the SN and galaxy move to the other detector), on the other hand, produces a very clean sky image. The disadvantage is that sometimes the sky may be taken as much as 15 minutes before or after the SN+galaxy exposure, and the NIR sky can change over this time. Thus the sky images, while very clean, may have larger residual subtraction features because of changing sky emission levels.

On the photometric WIRC nights, we observed three to five standard stars from Persson et al. (1998) on detector 2. For observing efficiency, we based the photometric transformations to the standard system on data obtained with this single detector. Standard stars were observed with five dither positions and three repetitions at each position. We chose stars with J fainter than 11 mag to avoid saturation and fixed the exposure time of individual images to 5 s, resulting in total exposure times of 75 s for each filter. The photometric transformations derived from these observations were applied to comparison stars in the SN fields (observed only with detector 2) to obtain precise magnitudes for these local standards.

For our PANIC observations, we selected a slightly different pointing for each SN than that used for WIRC in order to include the maximum number of comparison stars in the smaller FOV of PANIC. Observations were made with five dither positions and two or three exposures per position, depending on the SN brightness. The exposure times for individual images were 10, 20, or 30 s, with total exposure times ranging between 100 and 450 s. We followed each of these sequences by a sky sequence after offsetting the telescope by $1'$ or $2'$ in any direction, making sure that the host galaxy fell outside of the sky field.

3.3. Spectroscopy

Our spectroscopic observations typically started during the afternoon by taking bias frames, followed by a series of dispersed dome flats with wide (~$7''$) and narrow (~$1''$) slits. In addition, for the WFCCD and LDSS-2 instruments, dome flats were obtained for the respective imaging filters (*BVI* for the WFCCD and *BVR* for LDSS-2). We adjusted the lamp voltage and the exposure times to obtain 10,000 e^- pixel^{-1} in our flat-field direct images and a maximum of 15,000 e^- pixel^{-1} in the spectroscopic flats.

We observed SNe with the narrow slit aligned along the parallactic angle (Filippenko 1982) according to a priority list built for every night. Total exposure times with the WFCCD and the Modular Spectrograph varied between 900 and 2700 s, and between 180 and 900 s with LDSS-2. For each SN, we divided the total exposure into three independent integrations for cosmic-ray rejection. In between the first two or last two exposures, an image of a comparison lamp for wavelength calibration was taken. During the night we observed at least two spectrophotometric standards (Hamuy et al. 1992, 1994a) with the wide slit. A few weeks after the beginning of the first campaign, we decided to include one observation per night of a telluric standard (Bessell 1999) with high S/N and the same narrow slit used for the observations of the SNe. Since data from the CTIO 1.5 m telescope were obtained in service mode, we were not able to obtain such a calibration with that instrument.

4. DATA REDUCTION

4.1. Optical Imaging

To accelerate and automate the reduction of the optical imaging, we developed a custom IRAF[7] script package to handle the Swope 1 m data. For all nights, we first corrected the exposure time for the shutter timing error (see Appendix A). Next we processed the images through bias subtraction, nonlinearity corrections (see Appendix B), and flat-field division. For a given filter, we constructed the flat field by dividing the median-filtered combined sky flat by the median-filtered combined dome flat, heavily smoothing this ratio, and multiplying this illumination correction into the dome flat. This procedure removed a small gradient of ~1%. When a nightly sky flat could not be obtained we used one from a previous night. Random checks of science images taken during the night typically showed that the sky level across the images varied by less than 1%. Although fringing is present in the i' band we did not attempt to remove it from our frames. Since our i'-band instrumental magnitudes of the local standards in the SN fields can be transformed to the standard system (as explained below) to better than 0.015 mag, this implies that neglecting the fringing correction introduces an error of $\lesssim$0.015 mag.

Next we used the IRAF DAOPHOT package to compute instrumental magnitudes for the standard stars with an aperture of $7''$ in radius (the same used in the establishment of the standard system) and a sky annulus located $7''$–$9''$ from the star. We computed instrumental errors using a Poisson model based

[7] IRAF is distributed by the National Optical Astronomy Observatory, which is operated by the Association of Universities for Research in Astronomy, Inc., under cooperative agreement with the National Science Foundation.

on the noise parameters of the CCD. This model provided realistic errors for faint stars but excessively small errors for bright stars. We adopted 0.015 mag as the floor to the calculated errors, based on the observed dispersion in the transformation between instrumental and standard magnitudes of bright stars (see below). To derive the transformation of the instrumental magnitudes into the standard system, we used the following (Harris et al. 1981):

$$u' = u - k_u x_u + \mathrm{ct}_u(u - g) + \mathrm{zp}_u, \quad (1)$$

$$g' = g - k_g x_g + \mathrm{ct}_g(g - r) + \mathrm{zp}_g, \quad (2)$$

$$r' = r - k_r x_r + \mathrm{ct}_r(r - i) + \mathrm{zp}_r, \quad (3)$$

$$i' = i - k_i x_i + \mathrm{ct}_i(r - i) + \mathrm{zp}_i, \quad (4)$$

$$B = b - k_b x_b + \mathrm{ct}_b(b - v) + \mathrm{zp}_b, \quad (5)$$

$$V = v - k_v x_v + \mathrm{ct}_v(v - i) + \mathrm{zp}_v. \quad (6)$$

In these equations $u'g'r'i'BV$ (left-hand side) are the published magnitudes in the standard system (Landolt 1992; Smith et al. 2002), *ugribv* (right-hand side) correspond to the natural-system magnitudes, k_i is the extinction coefficient, x_i is the effective air mass, ct_i is the color term, and zp_i is the zero point for filter *i*.

At the beginning of the first campaign, we observed a standards field hourly (~20 stars during the night), which allowed us to solve for all unknowns (ct_i, zp_i, k_i). As the campaign progressed the pressure to observe SNe increased, leaving less time for measurements of standards. We adopted the approach of measuring only five to eight standard stars over a wide range of air mass (~10 stars during the night). With this small number of stars we fixed the color term to the average value, solving only for the extinction coefficient and zero point.

During the first observing campaign, we obtained weighted least-squares solutions for 53 clear nights. Dispersions around best-fit transformations were ~0.02–0.04 mag in u' and ~0.01–0.02 mag in other filters. This clearly demonstrates the excellent quality of the LCO site for this photometric program. Figure 3 shows the extinction coefficients as a function of time for all filters. While the scatter was only ~0.03 in $g'r'i'BV$, the dispersion was 3 times greater in the u' band, which is the most sensitive to extinction variations from night to night.

Color terms are presented in Figure 4. No obvious secular change was seen over this 250 day span in any filter, even though the primary mirror was washed on 2005 April 6 UT. While the color terms were close to zero ($\lesssim$0.02) for $g'r'i'$, the magnitudes of these terms in $u'BV$ were greater (~0.04–0.06), indicating small but nonnegligible differences between the instrumental and standard system.

To calibrate the local standards around the SN, we started by selecting the 5–10 brightest stars in every SN frame. For each frame, we used these stars to compute aperture photometry and derive the magnitude correction between a small aperture (generally 3″) and the 7″ aperture employed for the Johnson+SDSS standards. The aperture correction was typically ~0.03–0.1 mag. We assumed there were no field effects in the aperture corrections. Then we computed photometry for 10–15 field stars through the small aperture and corrected to the large aperture, bringing the natural-system photometry to the 7″ radius aperture. While this correction added some complication to the procedure, it improved the statistical accuracy of the fainter stars.

Finally, we used equations (1)–(6) to derive magnitudes in the standard system for the local standards. The uncertainty in the resulting magnitudes was the Poisson error in the instrumental magnitudes (assuming a minimum error of 0.015 mag). Here we neglected the uncertainty in the aperture correction, which was always less than 0.01 mag (otherwise we excluded such measurements). From the multiple measurements obtained on different clear nights we took weighted averages, yielding a photometric sequence of secondary standards around each SN with uncertainties as small as 0.004 mag in the individual magnitudes.

We then performed differential photometry of the SN relative to the local standards. The great advantage of this approach is that, since the SN is observed simultaneously with the field stars, the magnitude differences within a CCD frame are, to first order, immune to the passage of clouds. To improve the instrumental precision, we performed point-spread function (PSF) photometry. For this purpose, we employed all the stars of the photometric sequence to determine an average PSF for every CCD image, and we fitted the resulting PSF to the SN and the standards to a radius of 3″. We converted the instrumental magnitudes to the standard system using equations (1)–(6), assuming that the extinction effects ($k_i x_i$) were simple additive constants that were absorbed, to first order, by the zero point. As shown in Figure 4, the color terms had no secular variations and we adopted average color terms, solving only for the photometric zero points. The final uncertainty in the SN magnitude was the instrumental error in the PSF fit (assuming a minimum of 0.015 mag, as explained above). We neglected errors due to the transformation to the standard system since the uncertainty in the color term and in the zero point are well below 0.015 mag.

The extraction of the SN magnitude from a CCD frame is generally uncertain because the SN resides in a host galaxy with unknown features at the SN position. Thus, the light curves computed so far should be considered preliminary. As soon as we obtain galaxy templates with the 2.5 m telescope, we will

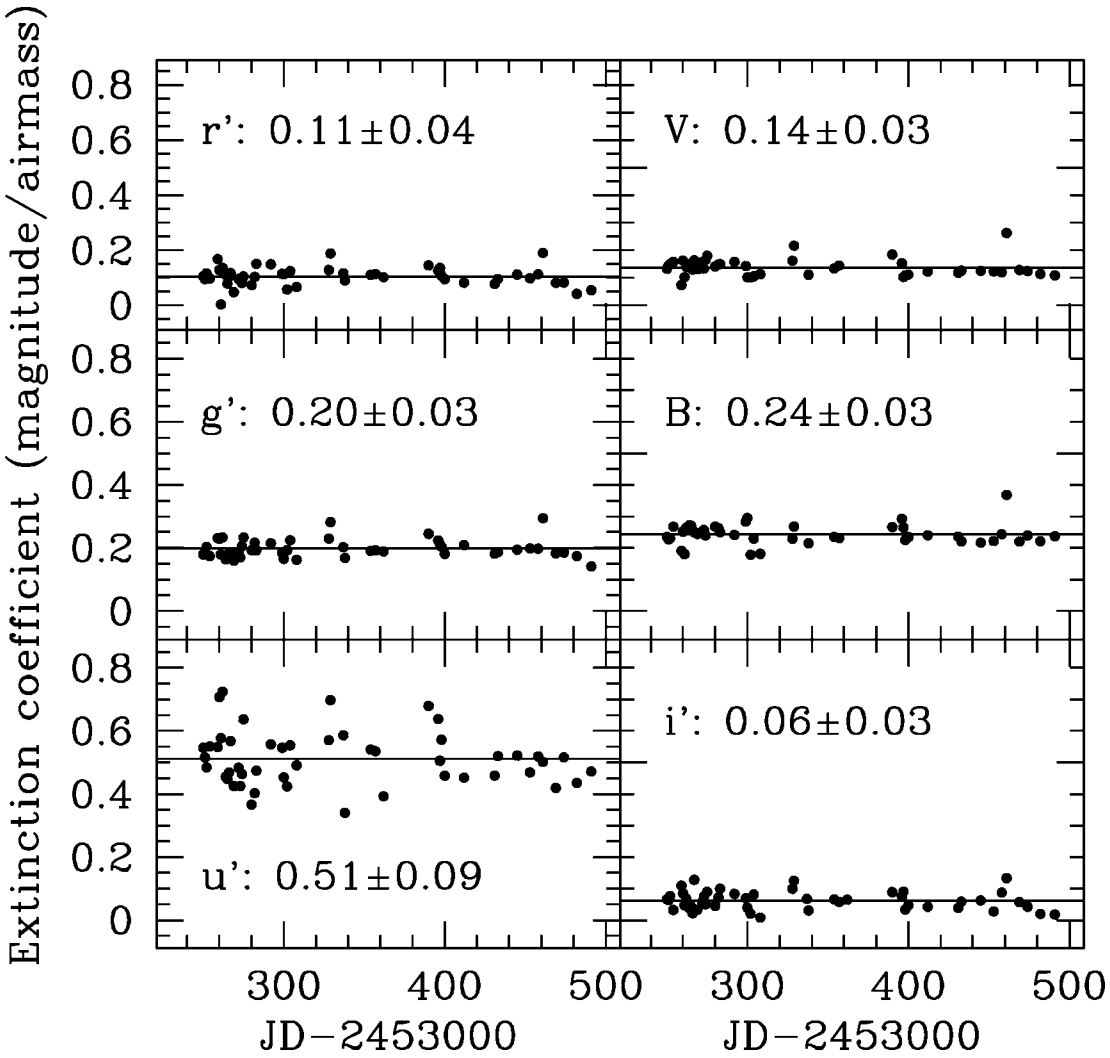

FIG. 3.—Extinction coefficients for the $u'g'r'i'BV$ filters as a function of time. The average coefficient is plotted with a horizontal line, and its numerical value is indicated in each panel, along with the rms scatter.

use image subtraction to remove the image of the galaxy and obtain definitive light curves. This procedure will follow that described by Hamuy et al. (1994b), which consists of (1) using the task `geomap` to determine the coordinate transformation between the two images (assuming a two-dimensional linear polynomial) and using the task `geotran` to register the template to the SN+galaxy image; (2) using the task `psfmatch` to find the two-dimensional difference kernel that, when convolved with the template, matches the PSF of the SN+galaxy image; (3) using the task `linmatch` to match the flux scale of the template to that of the SN+galaxy image; (4) subtracting the modified template from the SN+galaxy image; and (5) extracting a small box around the SN from the subtracted image and inserting it in the original SN+galaxy image.

The custom script package developed for the Swope telescope was used also to process the WFCCD and LDSS-2 data through the flat-field division. We have not attempted yet to compute SN magnitudes for these instruments because the lack of standard observations has prevented us from calculating color terms. This will be remedied during the second campaign.

4.2. Infrared Imaging

We reduced both WIRC and PANIC data using software pipelines. These pipelines are a combination of IRAF scripts following the steps of (1) linearity correction, (2) dark combination and subtraction, (3) flat-field combination and division, (4) bad-pixel mask production, (5) sky image computation and subtraction, and (6) combination of dithered frames into final stacked images. Both pipelines work in a similar fashion, with slight differences due to differing observing procedures.

In the first step, we applied a predetermined linearity cor-

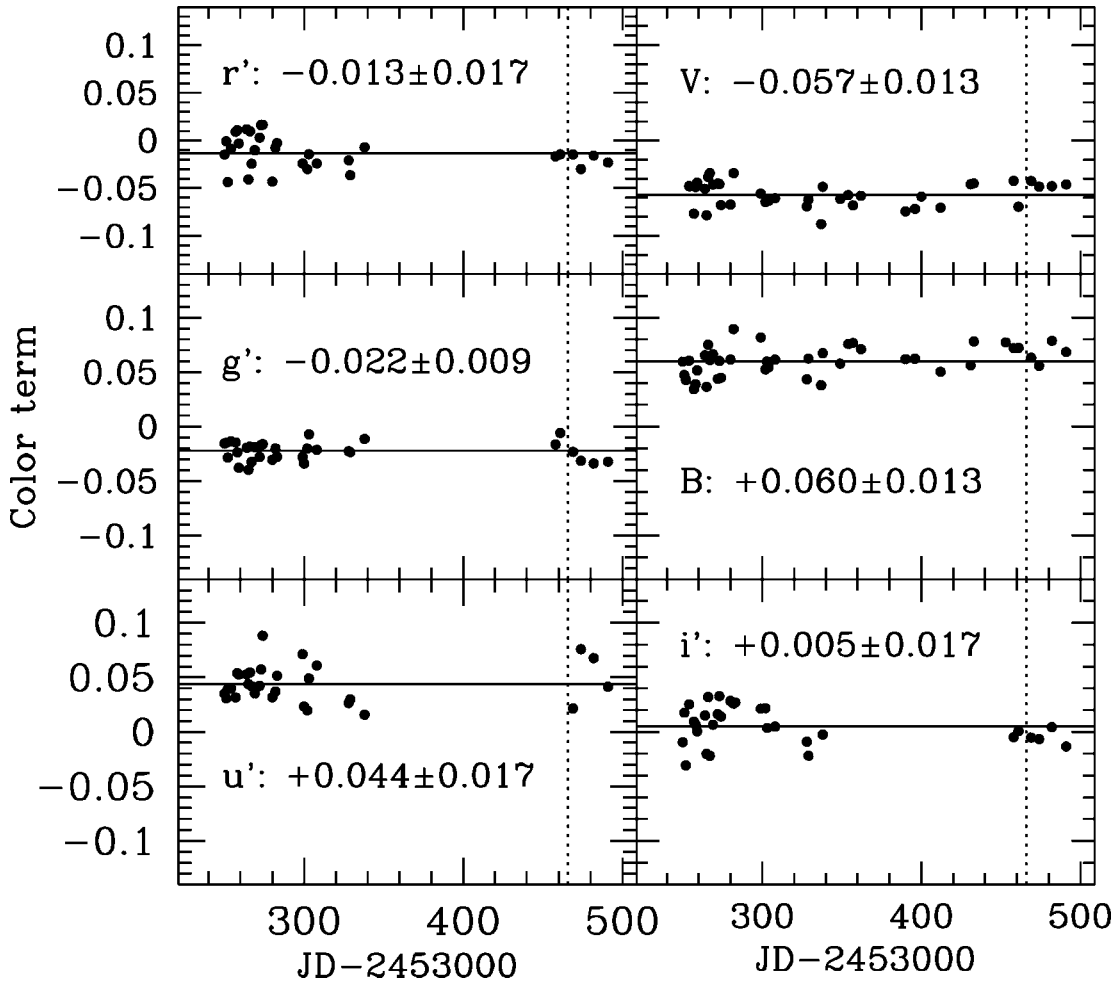

FIG. 4.—Color terms for the $u'g'r'i'BV$ filters as a function of time. The average color term is plotted with a horizontal line, and its numerical value is indicated in each panel, along with the rms scatter. The vertical dotted line shows the time when the primary mirror of the 1 m telescope was washed.

rection law for the HAWAII-1 detectors to every pixel value above 16,000 e^-:

$$I_{\rm corr} = c_0 + c_1 I + c_2 I^2, \tag{7}$$

where I is the observed number of ADUs, $I_{\rm corr}$ is the corrected value, and the coefficients are set to $c_0 = 4.291443 \times 10^1$, $c_1 = 9.752524 \times 10^{-1}$, and $c_2 = 1.962545 \times 10^{-6}$. Next, we normalized the dark-subtracted dome flats by the median. We considered pixel values outside the range 0.6–1.67 to be unrealistic, replacing them by 1 in the normalized flat and marking them in the nightly bad-pixel mask. If sky flats were taken (as was usually the case for PANIC), we median combined them and normalized the result to an average value of 1.0, replacing pixel values outside the range 0.2–5 by 1. We checked the results for possible residual stars. In the case of WIRC, we preferred sky flats (when available) to dome flats and we used them to check the illumination quality of the latter, which was usually good to within 1% for all filters. In the case of PANIC, dome flats showed illumination gradients of about 5%–10% across the image. Therefore, when sky flats could not be obtained, we used ones from a previous night. We stored all combined darks, flats, and bad-pixel masks of a night for future use or examination.

Sky frames to be subtracted from individual object frames were then constructed. We combined off-target images to produce sky frames in a two-step process. First, we computed a sky frame by directly averaging all off-target images. We subtracted this first sky frame from the individual off-target images. We detected objects in the subtracted frames and masked them in the original frames. We recalculated the sky frame, scaling the images to a common mode. We scaled the sky to the mode of the individual (dithered) object frames and subtracted it from them. We computed also the mode of the object frame in a two-step process to eliminate the contribution of sources in the image. We obtained the final image by aligning and averaging

the individual object frames. In this process, we preserved all pixels except those marked in the bad-pixel mask. Because the images may have been taken in nonphotometric conditions, we trimmed the data to only the regions of complete overlap. We generally obtained two images per SN and filter with WIRC (one from detector 2 and another from detector 3), and one image with PANIC.

Once the pipelines had produced stacked science images, we proceeded with the photometric measurements. Every time standard stars were observed with WIRC, we measured instrumental magnitudes through a standard aperture of 5″ in radius (Persson et al. 1998), with a sky annulus at 5″–7″ from the star. The magnitudes carried associated statistical uncertainties based on a Poisson model of the noise. As with the optical photometry, these estimates turned out to be unrealistically small when the objects were bright. Based on the dispersion found in the photometric solutions (see below), we estimate the minimum error in a single measurement to be 0.02 mag. This was our adopted minimum uncertainty in the instrumental magnitudes.

We used the instrumental magnitudes of standard stars to solve for the photometric transformation of the night, defined by the following equations:

$$Y = y - k_y x_y + \mathrm{zp}_y, \tag{8}$$

$$J = j - k_j x_j + \mathrm{zp}_j, \tag{9}$$

$$H = h - k_h x_h + \mathrm{zp}_h, \tag{10}$$

$$K_s = k - k_k x_k + \mathrm{zp}_k. \tag{11}$$

Here $YJHK_s$ are the magnitudes in the standard system (the JHK_s magnitudes published by Persson et al. [1998] and the Y magnitudes given in Appendix C), $yjhk$ are the corresponding instrumental magnitudes, k_i is the extinction coefficient, x_i is the effective air mass, and zp_i is the zero point for filter i. We fixed the extinction coefficients for JHK_s to the canonical values given by Persson et al. (1998): $k_j = 0.1$, $k_h = 0.05$, and $k_k = 0.08$. In the case of Y, we used the same value as for J ($k_y = 0.1$). We employed a weighted least-squares method to find the zero points zp_i. Typical dispersions around the fits were ~0.02–0.03 mag for all filters. On six nights, we observed 4–5 standards spread over air mass 1–2 in order to also fit the extinction coefficients. We found no significant deviations from the nominal values for JHK_s. In the Y band we found an average of $k_y = 0.06 \pm 0.01$, in agreement with the value of $k_y = 0.047$ given by Hillenbrand et al. (2002).

Note that we assumed zero color terms since the instrument detector and filters were essentially the same as in Persson et al. (1998). We will verify and monitor this assumption during the course of future campaigns.

With the photometric solution for the night, we proceeded to calibrate the local standard stars in each SN field observed with detector 2 of WIRC. We started by measuring magnitudes of bright, isolated stars through apertures of 1″–5″ in every stacked science frame and deriving the magnitude correction between a 2″ and a 5″ radius aperture. Typical aperture corrections ranged between 0.02 and 0.1 mag. We kept this correction below 0.1 mag by increasing the size of the small aperture, if necessary. Since the uncertainty in the aperture correction was generally ~0.02 mag, the increase in the statistical uncertainty on the 2″ measured magnitude was marginal and certainly lower than that introduced by increasing the aperture to 5″. We measured magnitudes for a number of comparison stars (between 3 and 15) in each SN field through the small aperture and corrected them to the 5″ aperture. We transformed these instrumental magnitudes to the standard system using equations (8)–(11). The weighted average of the resulting magnitudes for all comparison stars obtained on different photometric nights was calculated and checked for consistency. We then computed SN magnitudes relative to comparison stars in a manner identical to that used for the optical data.

4.3. Spectroscopy

The first step in the spectroscopic reductions was to combine the bias and flat-field images and then process the science frames through overscan subtraction, trimming, bias correction, and flat-fielding. Next, a general wavelength calibration was derived for the night, which we used later as a starting point to obtain specific calibrations from the comparison lamp images obtained at the position of each SN. Our wavelength calibrations were typically characterized by an rms scatter of 0.1 pixel.

The sensitivity function for the night was then calculated. This procedure consisted of extracting one-dimensional spectra of the flux standards, applying the wavelength calibration, dividing them by the one-dimensional telluric standard spectrum (after eliminating by hand the weak intrinsic spectral features of such stars), and calculating a response curve based on the flux values measured for the standard stars. As pointed out by Bessell (1990; see also Matheson et al. 2000), the division by the telluric spectrum has the following advantages: (1) it effectively removes the high-frequency (10–250 pixel wavelength) wiggles in the spectrum that are introduced by typical flat-field continuum sources and that can have a higher frequency than the flux point spacing, especially in the red; (2) the response curve can be fit accurately with a low-order function; and (3) most of the telluric features disappear, except those which are strongly saturated (like the oxygen band near 7600 Å). The latter effect is very important in revealing the calcium, oxygen, and carbon features in the red.

Extraction of the SN spectra was accomplished using a window whose width was chosen depending on the seeing and the uniformity of the underlying galaxy distribution. Typically the window included ~90% of the SN flux and excluded the wings of the stellar profile where the contribution of the galaxy introduced unwanted noise. We used two adjacent windows along the spatial direction to estimate the sky level and the contri-

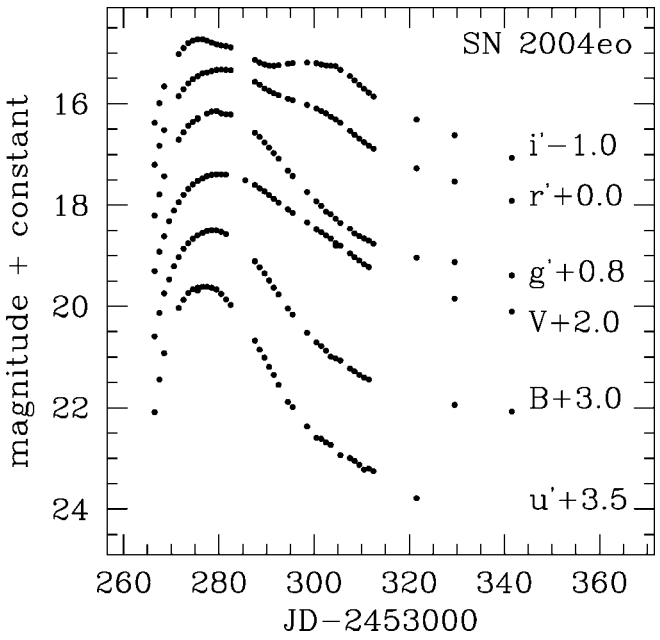

FIG. 5.—The $u'g'r'i'BV$ light curves of the Type Ia SN 2004eo.

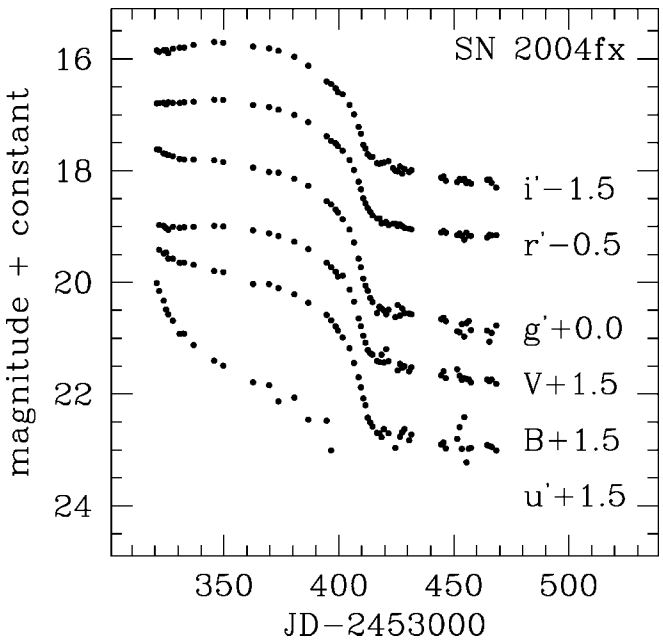

FIG. 6.—The $u'g'r'i'BV$ light curves of the Type II-P SN 2004fx.

bution of the galaxy in the SN aperture. In general, we tried to select these background windows as close as possible to the SN aperture, but the criteria for their selection varied from case to case depending on the nature of the adjacent background. A cubic spline was used to interpolate the background at the SN position. In most cases this interpolation provided an accurate estimate of the actual background, but occasionally the background was so nonuniform that some contamination of the host galaxy in the one-dimensional SN spectrum was unavoidable.

The extracted one-dimensional SN spectrum was then wavelength calibrated using the comparison lamp exposure taken at the SN position. Finally, the wavelength-calibrated spectra were divided by the one-dimensional telluric spectrum, and the sensitivity function was applied. Multiple observations of the same SN were combined into a final spectrum using a median-filter algorithm to remove deviant pixels caused by cosmic rays.

5. FIRST RESULTS

During the first low-z CSP campaign, we observed a total of 72 SNe. However, only 38 of these (17 SNe Ia, 12 SNe II, and 9 SNe Ibc) eventually qualified for inclusion in our follow-up program. This number represents 76% of our nominal expectation of ~50 SNe, with the difference being ascribed to natural variations in the year-to-year SN discovery rates.

5.1. Optical Imaging

During the first campaign, we obtained 7852 science optical images and established photometric sequences around all of the 38 SNe included in our follow-up observations. Final light curves must await the eventual subtraction of template images, but we present here preliminary light curves obtained with the Swope telescope of two SNe that did not suffer significant contamination from their hosts. While we chose these SNe for minimal contamination, the effect is bound to appear at some point when the SNe became very faint. Nevertheless, these examples illustrate the excellent photometric quality of the CSP light curves.

Figure 5 shows the $u'g'r'i'BV$ light curves of the Type Ia SN 2004eo. We observed this object for ~80 days starting ~10 days before maximum light with a cadence rarely achieved in previous studies. To estimate the precision of our photometry we fit a Légendre polynomial to the light curves with the lowest possible order but making sure to eliminate systematic residuals. In this case, the scatter around the fits amounts to 0.028 (order 8), 0.012 (order 9), 0.006 (order 12), 0.012 (order 15), 0.010 (order 9), and 0.008 (order 10) mag in u', g', r', i', B, and V, respectively. These dispersions can be taken as an empirical and realistic estimate of the random error in a single observation.

In Figure 6 we present optical light curves for the Type II plateau SN 2004fx. A prediscovery image on 2004 October 22, where the SN was not visible, indicates that the SN was caught no later than 20 days after explosion. Our first observations confirm that the SN was still quite blue at that point and that it grew progressively redder. We observed the SN on a weekly basis through the plateau phase for ~80 days, every other night for the next 20 days as it evolved faster, and less frequently again during the linear phase. The scatter in u' about a fourth-order Légendre polynomial is 0.10 mag, but this is dominated by the last few points where the statistical uncer-

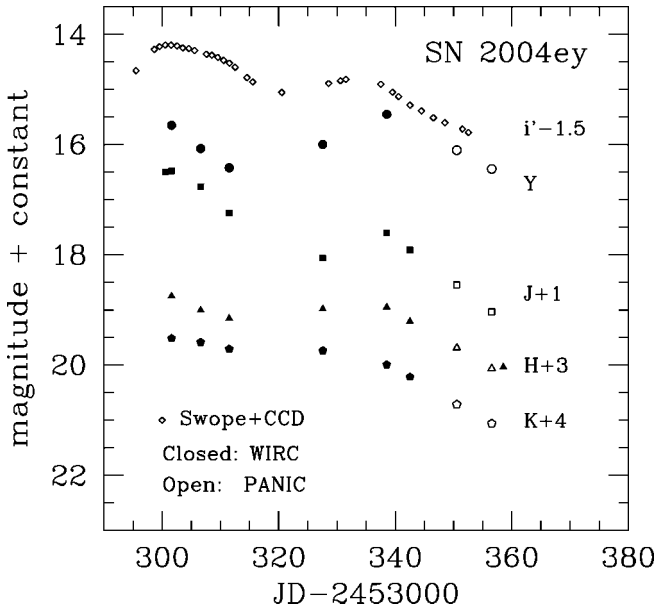

FIG. 7.—$YJHK_s$ light curves of the Type Ia SN 2004ey. The i'-band light curve is also shown to guide the eye.

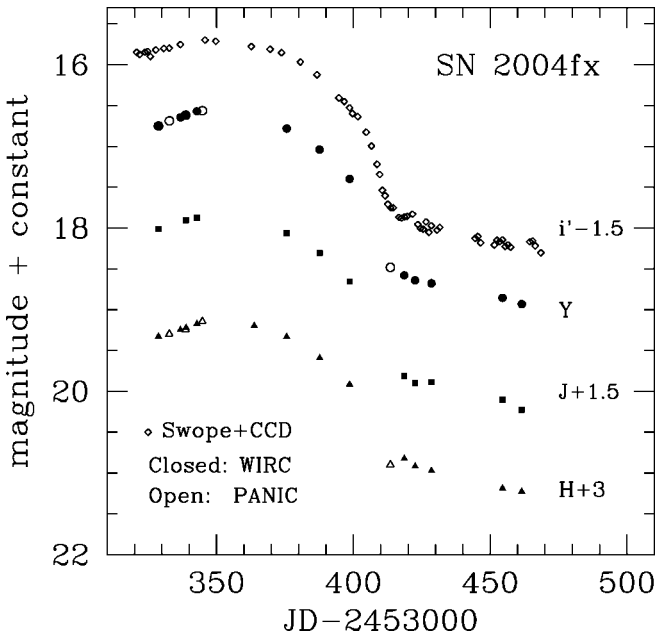

FIG. 8.—*YJH* light curves of the Type II-P SN 2004fx. The i'-band light curve is also shown to guide the eye.

tainties are much greater. When the four points with the greatest residuals are removed, the scatter drops to 0.044 mag. In the other bands, the scatter during the plateau phase around an order 10 Légendre polynomial varies between 0.02 and 0.03 mag. During the late-time linear phase the dispersion around a linear fit varies between 0.03 and 0.10 mag in $g'r'i'BV$. Part of this scatter is caused by variable amounts of galaxy contamination, as the seeing varied during the observations. We expect the final light curves to be much more uniform at these late epochs.

5.2. Infrared Imaging

During the first campaign, we obtained thousands of individual NIR images. The reduction process produced 1449 calibrated mosaics. We established photometric sequences around all of the 24 SNe included in our follow-up observations. Our NIR light curves are preliminary, awaiting the final template images and subtraction.

The NIR photometry is presented in the $YJHK_s$ light curves for two representative cases. Figure 7 presents the Type Ia SN 2004ey, while Figure 8 shows the Type II SN 2004fx. In both cases, we show for comparison the i'-band light curves from our own optical follow-up program.

The light curves show the typical sampling achieved of one point every 5–7 days, with gaps of up to 15 days during lunar "dark runs" when WIRC was not available at the 2.5 m du Pont telescope. By exchanging time with other programs, we were able to improve the sampling of some light curves, especially in the cases of SNe Ia around maximum light, to one point every 1–2 days. For SNe II, we relaxed the frequency of observations to one point every ∼10 days, enough to follow the slow plateau evolution. From the observations reduced independently for detectors 2 and 3 of WIRC, we are able to estimate the precision of the measurements. In cases of high S/N, where photon uncertainties can be neglected, the deviation between the two points is ∼0.02–0.03 mag in the *YJH* bands, consistent with expectations.

The distinctive secondary maximum of SNe Ia is clearly seen in Figure 7, occurring about 20 days after first maximum. This secondary maximum is remarkably prominent in *Y*, even surpassing the brightness of the first maximum. The NIR behavior of the Type II SN is characterized by a slow yet steady luminosity increase during the plateau phase, a feature previously seen in SN 1999em (Hamuy et al. 2001).

5.3. Spectroscopy

During the first CSP campaign, we obtained a total of 213 optical spectra that are fully reduced. During this period we provided spectral classification in the IAU Circulars for 27 SNe.

Figure 9 displays the spectroscopic evolution of the Type Ia SN 2004ef starting 8 days before maximum light for a period of 47 days. The telluric features are quite evident in these spectra because we did not obtain telluric standard observations for this SN.

Figure 10 shows the temporal evolution of the spectrum of the Type II SN 2004fx. Unlike the case for SN 2004ef, these spectra were divided by a telluric standard. Most telluric features disappear and only small residuals can be seen at the strongest absorptions (like the A band near 7600 Å).

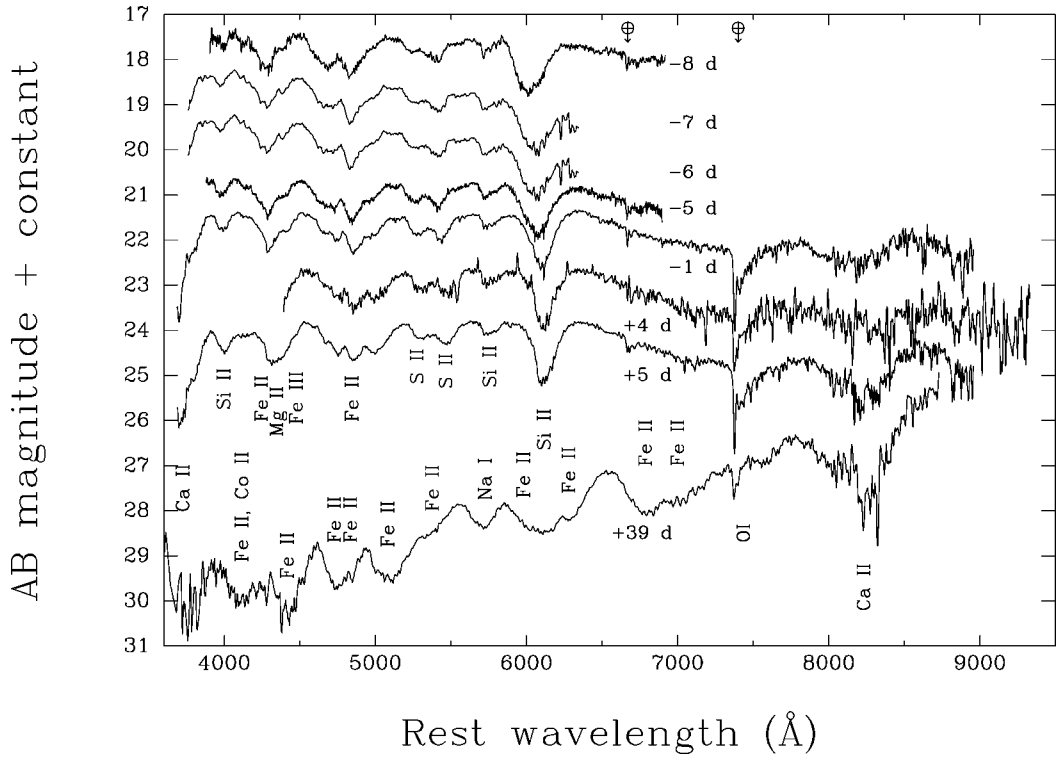

FIG. 9.—Spectroscopic evolution of the Type Ia SN 2004ef. The telluric features are indicated with the Earth symbol (⊕). AB mag $= -2.5 \log f_\nu - 48.6$ (Oke & Gunn 1983).

6. FUTURE IMPROVEMENTS TO THE CSP

In this paper, we have outlined the basic strategy of the CSP. In the second campaign, we will be modifying small aspects to improve the data quality still further.

The most important addition to the CSP will be RetroCam, a simple, high-throughput, NIR imager that will be mounted continuously on the Swope telescope during each SN campaign. It has a HAWAII-1 1024 × 1024 pixel HgCdTe detector and a single filter wheel containing *Y*, *J*, and *H* filters. Because it has no reimaging optics it does not operate in the K_s band. The scale is $0\farcs54$ pixel^{-1}, which is adequate for the image quality delivered by the telescope. RetroCam and the CCD camera (used for all the Swope measurements made so far) will both be mounted on a mechanical "swivel," such that they can be exchanged with each other in a matter of minutes. Typically this will be done during the afternoon, depending on SN scheduling requirements, weather, and so forth. Thus we expect to be able to alternate between $u'g'r'i'BV$ and *YJH* photometry every two or three nights or, in exceptional cases, during the same night. We expect that the final result will be light curves with comparable density of coverage from u' through *H*, and with sparser K_s coverage from WIRC and PANIC.

During the first campaign, we did not have enough engineering or cloudy time on our WIRC or PANIC nights to allow us to perform linearity tests. Hence, we have relied on the corrections that are given in the manuals of these facility instruments. We will improve this situation by carrying out our own tests during the second campaign.

During the first campaign, it was not always possible to achieve an optimal cadence of one spectroscopic observation every 5–7 nights per SN. We expect to improve this situation for future CSP campaigns by obtaining supplementary spectroscopic time on the CTIO 4 m and the European Southern Observatory NTT telescopes. Additional spectra will also be obtained at Lick Observatory.

7. SUMMARY AND CONCLUSIONS

The low-*z* program of the CSP is underway. During the first 9 month campaign, we were assigned 190 nights with the LCO 1 m telescope, 57 nights with the 2.5 m telescope, and a smaller number of nights with the two Magellan 6.5 m telescopes and the CTIO 1.5 m telescope. With this allocation, we were able to obtain follow-up photometry and spectroscopy for 38 SNe (17 SNe Ia, 12 SNe II, and 9 SNe Ibc).

In the first year of operation, we developed reduction pipelines and software that allowed us to produce optical+NIR light curves in real time and post them on our public Web site. Thanks to the nearly uninterrupted access to the Swope 1 m telescope, our optical light curves have an unprecedented gap-free temporal coverage. This data set constitutes the first ever

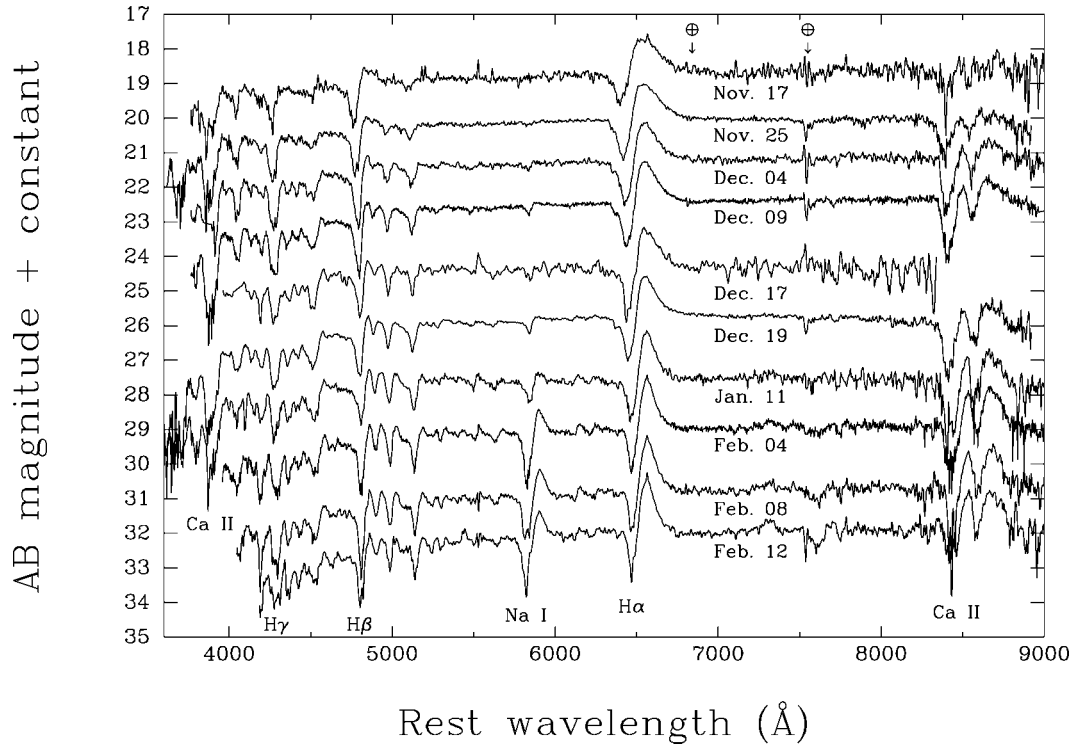

FIG. 10.—Spectroscopic evolution of the Type II-P SN 2004fx. The telluric features are indicated with the Earth symbol (⊕). AB mag $= -2.5 \log f_\nu - 48.6$ (Oke & Gunn 1983).

for SNe in the SDSS filters. Given that we used only one instrument and filter set, the light curves are very homogeneous in comparison to data sets in the literature such as the "gold sample" of Riess et al. (2004). Through careful attention to details, precisions of 0.03 mag in u' and 0.01 mag in $g'r'i'BV$ in single measurements have been achieved. We were able to sample the NIR light curves of SNe Ia every 5–7 days with longer gaps of 15 days during dark time, and those of SNe II every 10 nights. The precision of single measurements in the *YJH* bands was typically 0.02–0.03 mag, consistent with expectations.

Our data processing procedures allowed us to flux and wavelength calibrate hundreds of spectra in a timely manner. During the first campaign, the CSP provided spectroscopic types for 27 SNe. These spectra will serve as a valuable resource for improving *K*-corrections for SNe Ia and SNe II, as well as for measuring expansion velocities and line strengths in order to explore correlations with SN luminosities and thus refine the methods for distance determination.

We thank Janusz Kaluzny for providing linearity calibrations for the Swope CCD. This material is based on work supported by the National Science Foundation (NSF) under grant AST 03-06969. We also acknowledge support from *Hubble Space Telescope* grant GO-09860.07-A from the Space Telescope Science Institute, which is operated by the Association of Universities for Research in Astronomy, Inc., under NASA contract NAS5-26555. M. H. acknowledges support provided by NASA through Hubble Fellowship grant HST-HF-01139.01-A, and support from the Centro de Astrofísica FONDAP 15010003 and to Proyecto Fondecyt 1060808. A. V. F.'s group at UC Berkeley is supported by NSF grant AST 03-07894; he is also grateful for a Miller Research Professorship, during which part of this work was completed. KAIT was made possible by generous donations from Sun Microsystems, Inc., the Hewlett-Packard Company, AutoScope Corporation, Lick Observatory, the National Science Foundation, the University of California, and the Sylvia & Jim Katzman Foundation.

APPENDIX A

SHUTTER CORRECTIONS

For the curtain shutter design of the Swope 1 m telescope CCD camera, we expect a single constant error across the field. We attempted to measure this effect during several cloudy nights. With the dome closed, we adjusted the flat field lights until the illumination yielded 25,000 e^- pixel^{-1} in 30 s. The measurements consisted of taking one 30 s exposure, ten 3 s exposures without reading the CCD in between the individual exposures, and another single 30 s exposure. In the case of an additive shutter error t_s, the total effective exposure time for the two 30 s images was $30 + t_s$ s, while for the middle image the total effective exposure time was $10 \times (3 + t_s)$ s. The illumination ratio between the 10×3 s image and the average of the two 1×30 s images, r, was very close to 1, and we used it to solve for t_s from

$$t_s = \frac{30(r-1)}{10-r}. \qquad \text{(A1)}$$

In 2004 October, we determined t_s with the telescope pointed to four different positions without detecting significant differences. From 14 measurements we measured $t_s = 0.079 \pm 0.009$ (rms). We repeated this test four times during the campaign (with one telescope pointing), which yielded $t_s = 0.080 \pm 0.007$, 0.075 ± 0.009, and 0.077 ± 0.004, in agreement with the first test. On one night, we confirmed that t_s was an additive constant, independent of the exposure time. For this purpose, we took 10×4 s exposures bracketed by two 1×40 s images, which yielded $t_s = 0.083 \pm 0.003$, and 10×5 s exposures bracketed by two 1×50 s images, which yielded $t_s = 0.084 \pm 0.003$. These tests demonstrated that the shutter error was important, especially for short exposure times. For example, neglect of the correction would have introduced a 0.08 mag error in a 1 s exposure relative to a long one. Note that the uncertainty in this correction is only 0.002 mag in a 1 s exposure and proportionally less for longer exposures.

APPENDIX B

LINEARITY CORRECTIONS

When the sky was overcast, we used the Swope 1 m telescope to measure the linearity of the SITe CCD. With the dome closed during the night, we pointed the telescope to a white flat-field screen, adjusting the intensity of the quartz lamps to give 100 ADUs pixel^{-1} above the bias in 8 s. Then we took exposures of 4, 8, 16, 24, …, 1800 s, which allowed us to measure the CCD response between 50 and 23,000 ADUs pixel^{-1} (57,500 e^- pixel^{-1}), above which we noticed that the CCD became quite nonlinear. We bracketed each of these images with 8 s images in order to monitor the illumination drift of the quartz lamp. We found that the illumination could vary by up to ~2% during the 2 hr time span of the measurement sequence. Once we corrected the fluxes for these illumination variations, we fitted a model of the form

$$t_i + t_s = a_1 I_i \left(1 + a_2 \frac{I_i}{32{,}767} + a_3 \frac{I_i^2}{32{,}767^2}\right), \qquad \text{(B1)}$$

where I_i was the flux detected in t_i s.

The top panel of Figure 11 shows measurements obtained on 2004 October 6 (*filled circles*) and the best-fit model. The bottom panel shows the fractional residuals from the best fit. Although at low-illumination levels the residuals amount to ~2%, the cubic polynomial provides a reasonable fit to the CCD response over the whole dynamic range. A better fit would

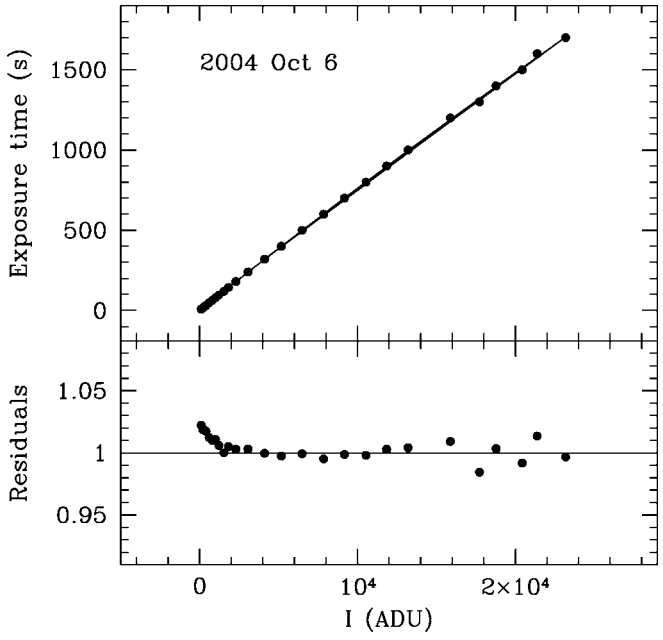

FIG. 11.—*Top*: Illumination per pixel vs. exposure time (corrected for shutter error) for the Swope SITe CCD (*filled circles*), measured on 2004 October 6. The solid line is a cubic polynomial model (see eq. [B1]). *Bottom*: Fractional residuals from the best fit.

have been obtained with a higher order polynomial, but we preferred to avoid an excessive number of free parameters in the model.[8] We then proceeded to linearize the observed fluxes on a pixel-by-pixel basis using the formula

$$I_{\rm corr} = I\left(1 + a_2\frac{I}{32{,}767} + a_3\frac{I^2}{32{,}767^2}\right). \qquad \text{(B2)}$$

The last four rows of Table 3 list the resulting coefficients from four different nights when we carried out these linearity measurements. Figure 12 shows the data obtained on 2004 October 6, along with the best-fit model (*solid line*). Note that the departures from linearity reached almost 6% at 23,000 ADUs, so it was absolutely necessary to correct the data for this effect to achieve high-precision photometry. Above this value the curve shown in Figure 12 has a steep upturn, so we find it safer to avoid illuminations above 23,000 ADUs and define our saturation limit at this value.

Included in Table 3 are previous measurements of the linearity of the SITe CCD carried out between 2001 May and 2004 May by J. Kaluzny. Two of these measurements are plotted in Figure 12. Note that the fits shown in Figure 12 represent the full range of the linearity corrections that have been measured for the SITe CCD. These differences are almost certainly due to errors in the measurements themselves rather than changes in the linearity of the detector. Hence, for the entire first campaign of the CSP, we adopted the correction measured on 2004 October 6, which lies in the middle of the range of fits. The uncertainty in this linearity correction translates to a maximum error in the photometry that is less than 2%.

TABLE 3
COEFFICIENTS FOR SWOPE SITe CCD LINEARITY CORRECTIONS

UT Date	a_2	a_3
2001 May	−0.1124	+0.0478
2001 Jul	−0.1596	+0.0926
2001 Sep	−0.1554	+0.0853
2002 summer	−0.1485 ± 0.0001	+0.0823 ± 0.0004
2003 May	−0.1573 ± 0.0006	+0.0924 ± 0.0006
2004 May	−0.1985	+0.1319
2004 Oct 6	−0.134 ± 0.009	+0.050 ± 0.009
2004 Nov 10	−0.138 ± 0.008	+0.056 ± 0.009
2005 Apr 22	−0.093 ± 0.013	+0.012 ± 0.014
2005 Apr 27	−0.139 ± 0.009	+0.061 ± 0.009

[8] We have empirically measured that the effect of adding a fourth-order term to the polynomial fit affects the SN magnitudes by $\lesssim$0.002 mag, thus demonstrating that this correction is unnecessary.

APPENDIX C

THE *Y*-BAND PHOTOMETRIC SYSTEM

In § 4.2 the *Y*-band photometric solution represents a special case, since Persson et al. (1998) only defined the standard JHK_s system. The *Y*-band system has been recently introduced by Hillenbrand et al. (2002). In order to derive *Y* magnitudes for all of the Persson et al. (1998) standard stars, we defined a relationship between the $(Y - K_s)$ and $(J - K_s)$ colors for a series of Kurucz model spectra.[9] These models have solar abundances and effective temperatures between 3500 and 10,000 K, thus producing a grid of spectra for main-sequence star analogs. We computed synthetic YJK_s magnitudes for each model using the total system transmission functions for PANIC shown in Figure 2. Figure 13 shows the resulting $(Y - K_s)$ versus $(J - K_s)$ diagram, together with the measurements published by Hillenbrand et al. (2002; their Table 2). The data from Hillenbrand et al. (2002) scatter significantly, but in general they follow the synthetic values for $(J - K_s) < 0.5$ mag. For 0.7 mag $< (J - K_s) < 1.2$ mag, there is a systematic difference of ~0.1 mag in $(Y - K_s)$ between the measurements and the models.

We decided to use the synthetic colors from the models to obtain a fifth-order polynomial fit of the form

$$(Y - K_s) = \sum_{i=0}^{5} a_i (J - K_s)^i, \qquad \text{(C1)}$$

where $a_0 = -0.017$, $a_1 = 1.901$, $a_2 = -1.296$, $a_3 = 2.289$, $a_4 = -2.409$, and $a_5 = 0.999$. The fit is shown in Figure 13 in the range of colors for the Persson et al. (1998) standards. We chose to ignore any zero-point difference and thus defined $(Y - K_s) = 0$ when $(J - K_s) = 0$ in order to maintain the original definition of α Lyr having 0.00 mag at all wavelengths (Elias et al. 1982). We therefore used the following formula to compute *Y*-band magnitudes from *J* and K_s for all of the Persson et al. (1998) standards:

$$\begin{aligned} Y = K_s &+ 1.901(J - K_s) - 1.296(J - K_s)^2 \\ &+ 2.289(J - K_s)^3 - 2.409(J - K_s)^4 \\ &+ 0.999(J - K_s)^5. \end{aligned} \qquad \text{(C2)}$$

As suggested by the referee, we recomputed *Y*-band magnitudes for the Persson et al. (1998) standards using the

[9] Main-sequence models with $T_{\rm eff}$ between 3500 and 10,000 K, $\log g = 4$, and solar abundances.

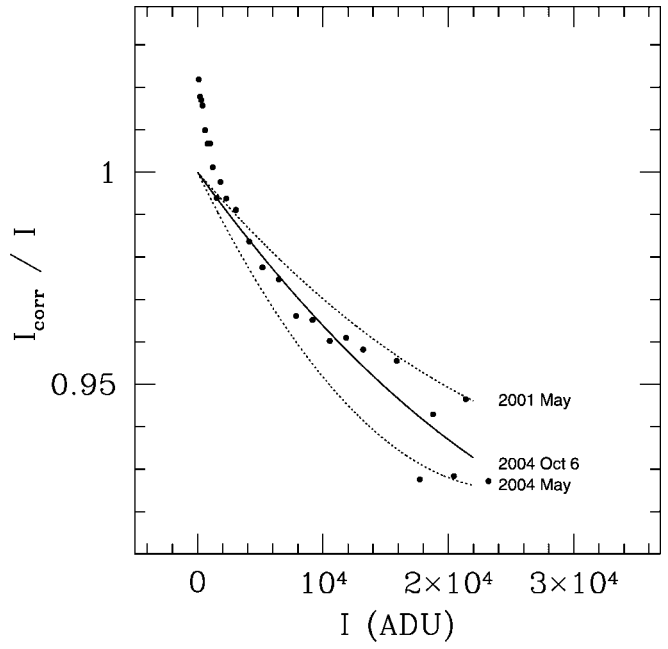

FIG. 12.—Nonlinear correction for the Swope SITe CCD as a function of the number of detected ADUs. The points show the data we obtained on 2004 October 6, and the solid line shows the best-fit model. The two fits shown with dotted lines were found by J. Kaluzny prior to the CSP (2001 May and 2004 May). These fits were chosen to represent the full range of corrections that have been measured for the SITe detector.

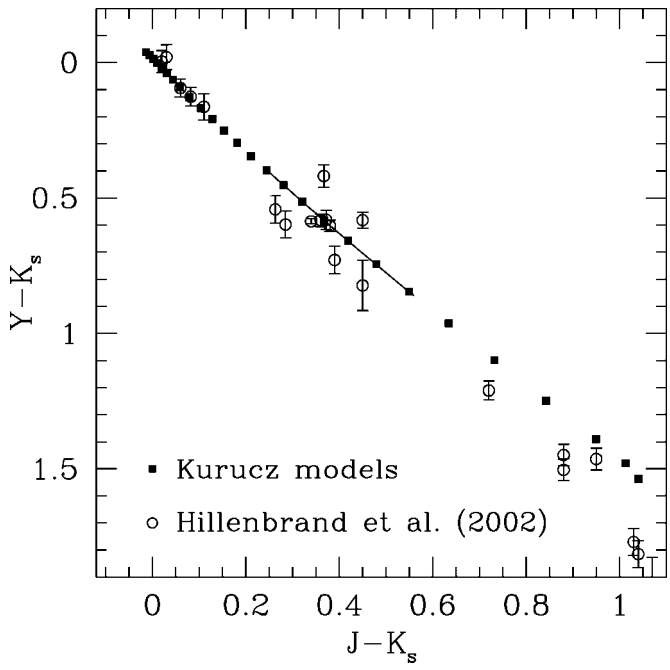

FIG. 13.—A $(Y - K_s)$ vs. $(J - K_s)$ diagram for a grid of main-sequence–analog Kurucz model atmospheres (*filled squares*), and measurements of standard stars published by Hillenbrand et al. (2002; *open circles*). The solid line shows a polynomial fit to the models drawn over the range of $(J - K_s)$ colors covered by the Persson et al. (1998) standard stars.

$(Y - J)$ versus $(J - H)$ relation yielded by the Kurucz models. The differences in the Y magnitudes obtained with both methods are never greater than 0.025 mag, and the mean difference is 0.006 ± 0.007 mag. We conclude that both approaches (Y from $Y - J$ and Y from $Y - K$) are valid and yield very similar results.

REFERENCES

Aldering, G. 2005, NewA Rev., 49, 346
Allington-Smith, J., et al. 1994, PASP, 106, 983
Bessell, M. S. 1990, PASP, 102, 1181
———. 1999, PASP, 111, 1426
Dessart, L., & Hillier, D. J. 2005, A&A, 439, 671
Eastman, R. G., Schmidt, B. P., & Kirshner, R. P. 1996, ApJ, 466, 911
Elias, J. H., Frogel, J. A., Matthews, K., & Neugebauer, G. 1982, AJ, 87, 1029
Filippenko, A. V. 1982, PASP, 94, 715
———. 2003, in From Twilight to Highlight: The Physics of Supernovae, ed. W. Hillebrandt & B. Leibundgut (Berlin: Springer), 171
———. 2005, in ASP Conf. Ser. 332, The Fate of the Most Massive Stars, ed. R. Humphreys & K. Stanek (San Francisco: ASP), 34
Filippenko, A. V., Li, W., Treffers, R. R., & Modjaz, M. 2001, in IAU Colloq. 183, Small Telescope Astronomy on Global Scales, ed. W.-P. Chen, C. Lemme, & B. Paczyński (ASP Conf. Ser. 246; San Francisco: ASP), 121
Folatelli, G., et al. 2006, ApJ, in press (astro-ph/0509731)
Foley, R. J., et al. 2003, PASP, 115, 1220
Freedman, W. L. 2005, in ASP Conf. Ser. 339, Observing Dark Energy, ed. S. C. Wolff & T. R. Lauer (San Francisco: ASP), 50
Fukugita, M., Ichikawa, T., Gunn, J. E., Doi, M., Shimasaku, K., & Schneider, D. P. 1996, AJ, 111, 1748
Gallagher, J. S., Garnavich, P. M., Berlind, P., Challis, P., Jha, S., & Kirshner, R. P. 2005, ApJ, 634, 210
Hamuy, M., & Pinto, P. A. 2002, ApJ, 566, L63
Hamuy, M., Suntzeff, N. B., Heathcote, S. R., Walker, A. R., Gigoux, P., & Phillips, M. M. 1994a, PASP, 106, 566
Hamuy, M., Trager, S. C., Pinto, P. A., Phillips, M. M., Schommer, R. A., Ivanov, V., & Suntzeff, N. B. 2000, AJ, 120, 1479
Hamuy, M., Walker, A. R., Suntzeff, N. B., Gigoux, P., Heathcote, S. R., & Phillips, M. M. 1992, PASP, 104, 533
Hamuy, M., et al. 1994b, AJ, 108, 2226
———. 2001, ApJ, 558, 615
Harris, W. E., Fitzgerald, M. P., & Reed, B. C. 1981, PASP, 93, 507
Hillenbrand, L. A., Foster, J. B., Persson, S. E., & Matthews, K. 2002, PASP, 114, 708
Jha, S. 2002, Ph.D. thesis, Harvard Univ.
Landolt, A. U. 1992, AJ, 104, 340
Leonard, D. C., et al. 2002, AJ, 124, 2490

Li, W., et al. 2000, in AIP Conf. Proc. 522, Cosmic Explosions, ed. S. S. Holt & W. W. Zhang (New York: AIP), 103
Martini, P., Persson, S. E., Murphy, D. C., Birk, C., Shectman, S. A., Gunnels, S. M., & Koch, E. 2004, Proc. SPIE, 5492, 1653
Matheson, T., et al. 2000, AJ, 120, 1487
———. 2005, AJ, 129, 2352
Oke, J. B., & Gunn, J. E. 1983, ApJ, 266, 713
Perlmutter, S., et al. 1999, ApJ, 517, 565
Persson, S. E., Murphy, D. C., Gunnels, S. M., Birk, C., Bagish, A., & Koch, E. 2002, AJ, 124, 619
Persson, S. E., Murphy, D. C., Krzeminski, W., Roth, M., & Rieke, M. J. 1998, AJ, 116, 2475
Phillips, M. M., Lira, P., Suntzeff, N. B., Schommer, R. A., Hamuy, M., & Maza, J. 1999, AJ, 118, 1766
Pritchet, C. J. 2005, in ASP Conf. Ser. 339, Observing Dark Energy, ed. S. C. Wolff & T. R. Lauer (San Francisco: ASP), 60
Riess, A. G., et al. 1998, AJ, 116, 1009
———. 2004, ApJ, 607, 665
Schmidt, B. P., Kirshner, R. P., Eastman, R. G., Phillips, M. M., Suntzeff, N. B., Manuy, M., Maza, J., & Avilés, R. 1994, ApJ, 432, 42
Smith, J. A., et al. 2002, AJ, 123, 2121
Stritzinger, M., et al. 2002, AJ, 124, 2100
Suntzeff, N. B. 2000, in AIP Conf. Proc. 522, Cosmic Explosions, ed. S. S. Holt & W. W. Zhang (New York: AIP), 65